Instabilities of the buoyancy layer for the Carreau fluid in thermally stratified medium

Bin Zhang, Moli Zhao, Yue Xiao,* and Shaowei Wang†
Department of Engineering Mechanics, School of Civil Engineering, and Shandong University, Jinan 250061, China

(Received 7 March 2023; accepted 6 July 2023; published 27 July 2023)

In this study, we consider the buoyancy-driven flow of a non-Newtonian fluid over an inclined flat plate immersed in a thermally stratified medium. Using the Carreau model, we determine the base flow profiles and associated linear stability results for both pseudoplastic and dilatant fluids. For steady basic flow, the shear-thinning behavior enhances the convection and heat transfer characteristics while it is opposite for shear-thickening flow. Based on linear stability analysis, the effects of Prandtl number, tile angle, and power-law index on the transverse traveling Tolmien-Schlichting waves, the stationary longitudinal rolls and the oblique rolls are investigated. Different from the Newtonian fluids, under appropriate parameters, a new oblique rolls mode appears in dilatant fluids. Furthermore, it is shown that both the TS mode and OR mode are destabilized and stabilized for shear-thinning and shear-thickening fluids, respectively. However, non-Newtonian effects always stabilize the SL mode. These results reveal that the nature of the stability depends on the rheological properties significantly.

DOI: 10.1103/PhysRevFluids.8.073904

I. INTRODUCTION

Natural convection in thermally stratified fluids is very common in many industrial processes and nature. The buoyancy-driven boundary layer (also known as *buoyancy layer*) flow will be generated when an inclined plate is heated in a stably stratified fluid. The inclined buoyancy layer is first introduced by Prandtl [1] to simulate the flows over valleys and mountains in stratified air. Based on a vertical buoyancy layer solution [2], Gill and Davey [3] investigated the linear stability of such a buoyancy layer at a vertical wall, and the inclined case was first analyzed by Iyer [4]. Two types of instabilities is identified: the transverse traveling Tolmien-Schlichting (TS) waves and the stationary longitudinal rolls (SL). Moreover, the nonlinear stability of inclined buoyancy layer with uniform-heat-flux wall is studied by Iyer and Kelly [5]. It is obtained that the bifurcation of inclined buoyancy layer can only be supercritical. Substantial progress has been made in many theoretical and numerical studies of Prandtl buoyancy layers [6–11]. Most of these studies are mainly focused on the transverse TS waves. Based on the three-dimensional stability analysis, Tao and Busse [12] demonstrated that the oblique roll (OR) mode will be more unstable than the transverse TS wave mode at some inclination angles and Prandtl numbers in ambient thermal stratification. In the inviscid frame, Candelier *et al.* [13] studied the three-dimensional stability of boundary layer flow in stable stratification. Besides, there are also some studies on convective and absolute instabilities. For example, the instabilities of free convection buoyancy layer for an isothermal vertical flat plate is studied by Krizhevsky *et al.* [14]. For the situation of the wall and the ambient fluid with

*xiaoyue@sdu.edu.cn
†shaoweiwang@sdu.edu.cn

different temperature gradients, Tao *et al.* [15,16] studied the temporal and spatial instability of the vertical buoyancy-driven flow from both theoretical and numerical aspects. More recently, the critical and spatiotemporal instability of the buoyancy-driven boundary layer on a vertical cylinder is investigated by Xiao *et al.* [17].

The above-mentioned objects of studies are all Newtonian fluids. In fact, buoyancy-induced flows with non-Newtonian behavior has also attracted considerable attention because it is very important in industrial applications, where it is common to deal with fluids such as molten plastics, mud, paint, blood and so on. In these problems, the most common fluids are pseudoplastic (shear-thinning) and dilatant (shear-thickening). For a review of the fundamental works, we refer to the paper by Siginer [18]. Generally, power-law model is the most commonly used to simulate the rheological behavior of non-Newtonian fluids. The model parameters usually have significant effects on the heat and mass transfer and stability of the flow. For example, the nature convection confined in an enclosure with non-Newtonian fluids is study by Ozoe and Churchill [19]. The rheological behavior is simulated by power-law model and it is observed that the critical Rayleigh number increases with the flow behavior index. Molla and Yao [20] investigated the natural convection of modified power-law viscosity model along a vertical flat plate. Their numerical results demonstrated that a similarity solution for natural convection exists near the leading edge. Kaddiri *et al.* studied the Rayleigh-Bénard convection of non-Newtonian power-law fluids with temperature dependent viscosity [21]. The numerical and analytical study of the onset of convection generated in a shallow cavity filled with power-law fluids is carried out by Alloui *et al.* [22]. They concluded that the onset of convection is subcritical for shear-thinning fluids and convection is found to occur at a supercritical Rayleigh number equals to zero for shear-thickening fluids.

Although power-law fluid has the advantage of simple use, it can not avoid the disadvantage of large viscosity when the shear rate is small. In 1972, Carreau model [23] was proposed to get around this problem. Subsequently, many theoretical and numerical studies based on the Carreau model have made substantial progress. Griffiths *et al.* [24] considered the stability of the non-Newtonian boundary layer flow over a flat plate with Carreau constitutive viscosity relationship. The results indicated that an increase in shear-thinning has the effect of significantly reducing the value of the critical Reynolds number. For the boundary layer flow over an inclined flat plate, Griffiths [25] presented the energy calculations to gain the mechanisms affecting the destabilization of the disturbances, and the results suggested that the effect of shear-thinning will act to stabilize the boundary-layer flow. Rousset *et al.* investigated the temporal stability of a Carreau fluid flow down an inclined plane [26]. It demonstrated that the critical parameter is lower for shear-thinning fluids than for Newtonian fluids and the shear dependency can change the nature of instability. Rayleigh-Bénard thermosolutal convection instabilities in an enclosure is numerically investigated by Rebhi [27]. A bistability convective phenomenon is discovered by performing the nonlinear asymptotic analysis.

Up to now, there is little research on the natural convection immersed in thermally stratified medium with non-Newtonian rheological behavior, although these are at the center of quite a few industrial applications. More importantly, it is still unknown how the tile angle and Prandtl number affect the instability in this buoyancy system, which is the main motivation of this paper. Different from the previous study, in this paper we will investigate the instability of an inclined buoyancy-driven flow with Carreau fluid in thermally stratified medium. The remainder of this investigation is outlined as follows. Section II describes the mathematical formulation of the fluid problem and the governing equations of linear stability analysis. The theoretical results of critical properties for three modes (TS waves, OR mode and SL mode) are described in Sec. III. Finally, conclusions and an outlook on further work are presented in Sec. IV.

II. MATHEMATICAL FORMULATION

Consider an inclined plate immersed in a quiescent ambient non-Newtonian fluid. A sketch of the geometry and the reference frame is shown in Fig. 1, where the plate is inclined at an angle

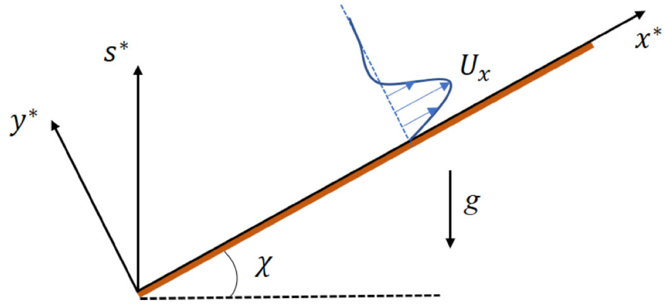

FIG. 1. Schematic geometry of an inclined plate immersed in thermally stratified fluid.

χ with respect to the horizontal. The coordinates x^* and z^* are parallel to the wall, which are the streamwise and spanwise directions of the plate. y^* is the coordinate in the wall-normal direction. The fluid in the far field is stably stratified and its temperature varies linearly in the vertical direction

$$T_\infty^*(s^*) = T_\infty^*(0) + N_\infty^* s^*, \tag{1}$$

where $T_\infty^*(0)$ is the reference temperature, N_∞^* is the temperature gradient in the medium, and s^* is the coordinate opposite to the direction of gravity $\mathbf{g}$. The subscript "∞" and the hyperscript "$*$" denote the ambient condition and dimensional quantities, respectively. The wall temperature is assumed to be $T_w^*(s^*) = T_\infty^*(s^*) + \Delta T^*$, where $\Delta T^* > 0$ is a constant temperature difference, i.e., the wall temperature is raised by a fixed amount ΔT^* above that of the fluid at the same height outside the buoyancy layer.

The governing equations with the Boussinesq approximation are

$$\begin{aligned}
\frac{\partial \mathbf{u}^*}{\partial t^*} + \mathbf{u}^* \cdot \nabla \mathbf{u}^* &= -\nabla\left(\frac{P^*}{\rho_r}\right) - \mathbf{g}\gamma(T^* - T_\infty^*) + \nabla \cdot \tau^*, \\
\frac{\partial T^*}{\partial t^*} + \mathbf{u}^* \cdot \nabla T^* &= \kappa \nabla^2 T^*, \\
\nabla \cdot \mathbf{u}^* &= 0,
\end{aligned} \tag{2}$$

where ρ_r is the reference density, γ is the coefficient of thermal expansion, κ is the thermal diffusivity, and τ^* is the stress tensor which is defined as

$$\tau_{ij}^* = 2\frac{\mu_a^*(S^*)}{\rho_r} D_{ij}^*. \tag{3}$$

Here, μ_a^* is the non-Newtonian viscosity, D_{ij}^* and S^* are the rate-of-strain tensor and the second invariant of the strain rate tensor, respectively, are given by

$$D_{ij}^* = \frac{1}{2}\left(\frac{\partial u_i^*}{\partial x_j^*} + \frac{\partial u_j^*}{\partial x_i^*}\right), \quad S^* = \sqrt{2D_{ij}^* D_{ij}^*}. \tag{4}$$

The non-Newtonian behavior of the fluid is described by the Carreau model. The constitutive equation is given by

$$\mu_a^* - \mu_\infty^* = (\mu_0^* - \mu_\infty^*)[1 + (\lambda^* S^*)^2]^{(n-1)/2}, \tag{5}$$

with μ_0^* the zero-shear-rate viscosity, μ_∞^* the infinite-shear-rate viscosity, λ^* the material time constant (relaxation time) and n the dimensionless power-law index. For many concentrated polymer solutions and melts, the infinite-shear-rate viscosity μ_∞^* is always associated with inviscid flows and is considered to be negligible (Bird *et al.* [28]) compared to the zero-shear rate viscosity μ_0^*. The fluid behavior is determined by λ^* and n. When $n = 1$, the Carreau model will degenerate into Newtonian fluid. For shear-thinning nature, we have $0 < n < 1$ and the fluid as a pseudoplastic fluid. And $n > 1$ indicates the fluid as a dilatant fluid.

We shall use dimensionless velocity, length, time, and temperature as defined by

$$u_0 = \frac{\rho_r d^2 g\gamma \Delta T^* \sin\chi}{\mu_0^*}, \quad d = \left(\frac{\mu_0^* \kappa}{g\rho_r \gamma \sin^2 \chi N_\infty}\right)^{\frac{1}{4}}, \quad \mathbf{u} = \frac{\mathbf{u}^*}{u_0},$$
$$(x, y, z) = \frac{(x^*, y^*, z^*)}{d}, \quad t = \frac{\mu_0^*}{\rho_r d^2} t^*, \quad T = \frac{T^* - T_\infty^*}{\Delta T^*}.$$

The nondimensional parameters of the problem are the Grashof number Gr, the Prandtl number Pr, and the dimensionless relaxation time λ:

$$\mathrm{Gr} = \frac{g\gamma \Delta T^* d^3 \rho_r^2}{\mu_0^{*2}}, \quad \mathrm{Pr} = \frac{\mu_0^*}{\rho_r \kappa}, \quad \lambda = \frac{u_0}{d}\lambda^*.$$

The nondimensional variables are $u_x = U_x + \tilde{u}_x$, $u_y = U_y + \tilde{u}_y$, $u_z = U_z + \tilde{u}_z$, $\mu_a = \mu_b + \tilde{\mu}_a$ and $T = \Theta + \tilde{\theta}$, where $\tilde{u}_x$, $\tilde{u}_y$, $\tilde{u}_z$, $\tilde{\mu}_a$, and $\tilde{\theta}$ are perturbations and U_x, U_y, U_z, μ_b, and Θ constitute the undisturbed basic flow solution.

Now, we will first derive the basic flow within the boundary layer induced by buoyancy. The flow is assumed to be steady and parallel in the following analysis. There must be $U_y \equiv U_z \equiv 0$, the velocity $U_x(y)$ and the temperature $\Theta(y)$ is directed in the x direction. The steady basic flow can be described by the following ordinary differential equations

$$\Theta + \mathcal{D}(\mu_b \mathcal{D} U_x) = 0, \tag{6a}$$
$$U_x - \mathcal{D}^2\Theta = 0, \tag{6b}$$

where $\mathcal{D} = \frac{\mathrm{d}}{\mathrm{d}y}$ and $\mu_b = [1 + (\lambda|\mathcal{D}U_x|)^2]^{\frac{n-1}{2}}$. The corresponding boundary conditions are

$$U_x(0) = U_x(\infty) = T(0) - 1 = T(\infty) = 0. \tag{7}$$

The above boundary value problem Eqs. (6) and (7) is solved by the built-in function `bvp4c` in MATLAB. It is worth noting that there are no explicit parameters of Grashof number, Prandtl number and tile angle in Eqs. (6) and (7), which means the steady basic flow is not relevant on Gr, Pr, and χ.

The velocity $U_x(y)$ and temperature $\Theta(y)$ profiles for different value of relaxation time λ and power-law index n are shown in Fig. 2. It is observed that the velocity and temperature variations for typical parameters are confined to the boundary layer at the wall. The flow reversals and temperature defects exist for both pseudoplastic fluid ($0 < n < 1$) and dilatant fluid ($n > 1$). The effects of power-law index n on basic flow are plotted in Figs. 2(a) and 2(b) for $\lambda = 4$. Larger n decreases the absolute values of the maximum and the minimum vertical velocity, and also decreases the temperature defect. The gradients of velocity and temperature profiles near the wall increases with the decreases of n, which indicates a thinning of the buoyancy boundary layer. This is to be expected physically, as the non-Newtonian viscosity becomes smaller, the flow will be more concentrated on the wall. Thus, compared to the Newtonian case ($n = 1$), the shear-thinning behavior ($0 < n < 1$) enhances the convection and heat transfer characteristics. The effects of material time constant λ on basic flow are plotted in Figs. 2(c) and 2(d) for shear-thinning flow $n = 0.8$. It is shown that large λ increases both the values of the maximum streamwise velocities and the temperature gradients near the wall. It is worth mentioning that the basic flow decays exponentially in the far-field, which can be obtained by logarithm of the absolute value of $U_x(y)$ or $\Theta(y)$. Theoretically, we can obtain the asymptotic analytical expression of velocity in the far-field. Considering that the velocity gradient in the far-field is very small, i.e., $\mu_b \approx 1$, Eqs. (6) become a system of linear equations. The analytical solution of the far-field velocity is $U_x(y) \sim e^{-\frac{y}{\sqrt{2}}} \sin(\frac{y}{\sqrt{2}})$, and the decay rate is $-1/\sqrt{2}$, which is consistent with the numerical solution.

Besides, the variation of the viscosity across the boundary layer is also presented in Figs. 2(e) and 2(f). It can be seen that the viscosity of shear-thinning fluid is lower than that of Newtonian fluid due to the velocity gradient in the boundary layer, but the viscosity of shear-thickening fluid

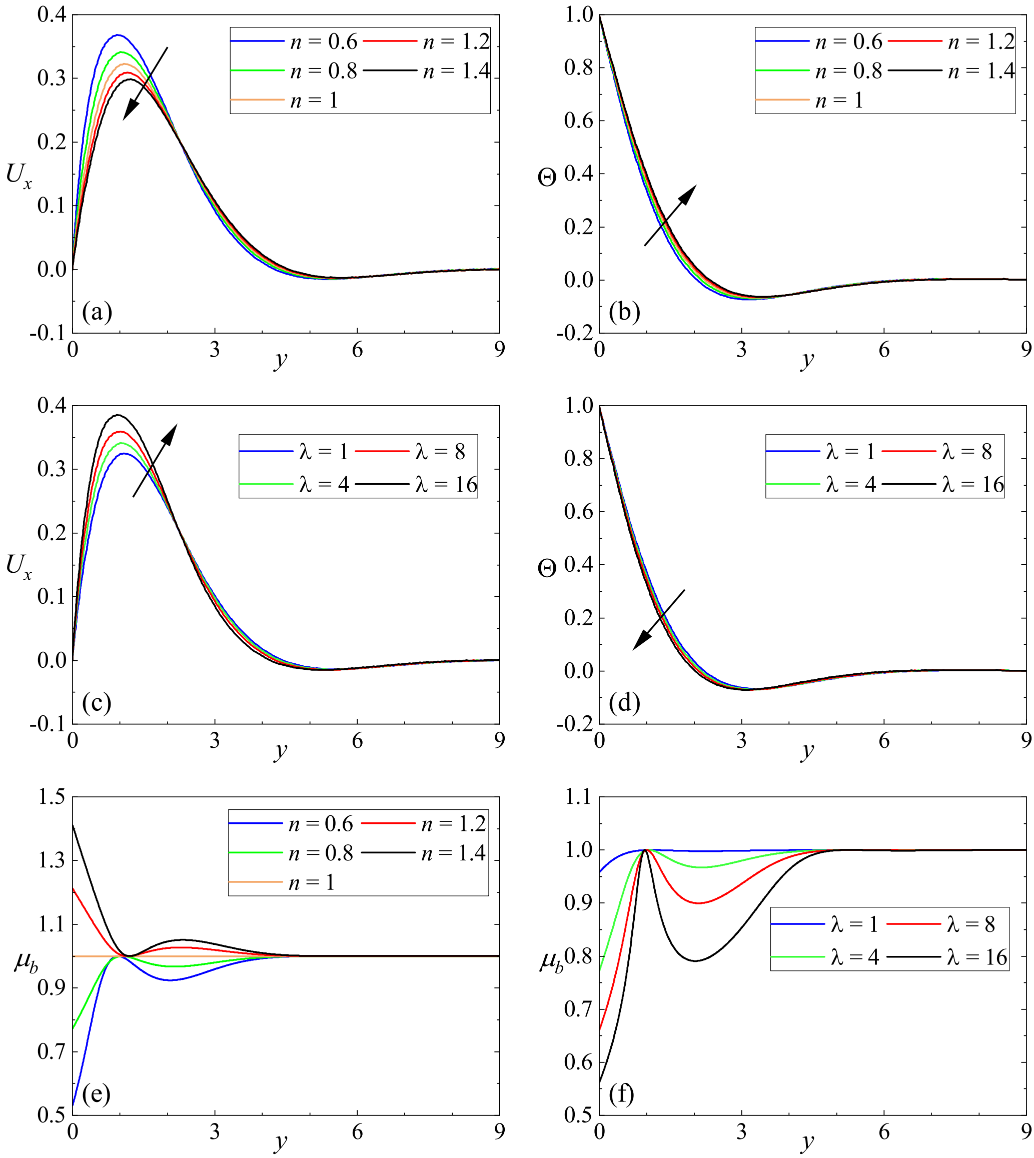

FIG. 2. The velocity profiles [(a),(c)] and the temperature profiles [(b),(d)] for different power index n and dimensionless relaxation time λ with fixing $\lambda = 4$ or $n = 0.8$. The black arrow indicates the direction in which the parameter increases. The variation of the viscosity across the boundary layer are presented in panels (e) and (f).

shows the opposite property. For shear thinning fluid ($n = 0.8$), the increase of relaxation time will promote the further reduction of viscosity. The flow field outside the boundary layer has almost no velocity gradient, and the viscosity is about 1.

In the following stability analysis, the general three-dimensional infinitesimal disturbances $\tilde{q}(x, y, z, t)$ on the base flow are decomposed into the form

$$\tilde{q}(x, y, z, t) = \hat{q}(y)\exp\left[\mathrm{i}(\alpha x + \beta y - \omega t)\right], \tag{8}$$

where α and β are the wave number in streamwise and spanwise directions, respectively. $\omega = \omega_r + \mathrm{i}\omega_i$ is the complex frequency. For linear stability analysis, $\tilde{\mu}_a$ is expanded by using the generalized binomial theorem and neglecting the high order nonlinear terms

$$\tilde{\mu}_a = [1 + (\lambda|\mathcal{D}U_x|)^2]^{\frac{n-3}{2}}[(n-1)\lambda^2\mathcal{D}U_x]\left(\frac{\partial \tilde{u}_x}{\partial y} + \frac{\partial \tilde{u}_y}{\partial x}\right). \tag{9}$$

The perturbation equations governing the stability of basic state are

$$\mathrm{i}\alpha\hat{u}_x + \mathcal{D}\hat{u}_y + \mathrm{i}\beta\hat{u}_z = 0, \tag{10a}$$

$$\mathcal{L}_1\hat{u}_x + \mathrm{Gr}\mathcal{D}U_x\hat{u}_y + \mathrm{i}\alpha\hat{p} = \hat{\theta} + \mu_2\mathcal{D}U_x(\mathcal{D}^2\hat{u}_x + \mathrm{i}\alpha\mathcal{D}\hat{u}_y) + (2\mu_2\mathcal{D}^2U_x + \mathcal{D}\mu_2\mathcal{D}U_x)(\mathcal{D}\hat{u}_x + \mathrm{i}\alpha\hat{u}_y), \tag{10b}$$

$$\mathcal{L}_1\hat{u}_y + \mathcal{D}\hat{p} = \cot\chi\hat{\theta} + 2\mu_2\mathcal{D}^2U_x\hat{u}_y + \mu_2\mathcal{D}U_x\mathrm{i}\alpha(\mathcal{D}\hat{u}_x + \mathrm{i}\alpha\hat{u}_y), \tag{10c}$$

$$\mathcal{L}_1\hat{u}_z + \mathrm{i}\beta\hat{p} = \mu_2\mathcal{D}^2U_x\hat{u}_y(\mathcal{D}\hat{u}_z + \mathrm{i}\beta\hat{u}_y), \tag{10d}$$

$$\mathcal{L}_2\hat{\theta} + \mathrm{Gr}\mathcal{D}\Theta\hat{u}_y + \frac{1}{\mathrm{Pr}}(\hat{u}_x + \cot\chi\,\hat{u}_y) = 0, \tag{10e}$$

where $\mathcal{L}_1$, $\mathcal{L}_2$, μ_1 and μ_2 are defined as follows:

$$\mathcal{L}_1 = -\mu_1(\mathcal{D}^2 - \alpha^2 - \beta^2) + \mathrm{i}\alpha\mathrm{Gr}U_x - \mathrm{i}\omega, \tag{11a}$$

$$\mathcal{L}_2 = -\frac{\mu_1}{\mathrm{Pr}}(\mathcal{D}^2 - \alpha^2 - \beta^2) + \mathrm{i}\alpha\mathrm{Gr}U_x - \mathrm{i}\omega, \tag{11b}$$

$$\mu_1 = [1 + (\lambda|\mathcal{D}U_x|)^2]^{\frac{n-1}{2}}, \tag{11c}$$

$$\mu_2 = [1 + (\lambda|\mathcal{D}U_x|)^2]^{\frac{n-3}{2}}[(n-1)\lambda^2\mathcal{D}U_x]. \tag{11d}$$

And the boundary conditions are given by

$$\hat{u}_x(0) = \hat{u}_y(0) = \hat{u}_z(0) = \hat{\theta}(0) = 0, \tag{12a}$$

$$\hat{u}_x(\infty) = \hat{u}_y(\infty) = \hat{u}_z(\infty) = \hat{\theta}(\infty) = 0. \tag{12b}$$

The stability of the steady-flow solutions with the boundary condition, Eqs. (10) and (12), constitute a generalized eigenvalue problem, given by the dispersion relationship

$$\mathcal{F}(\alpha, \beta, \omega; \mathrm{Gr}, \mathrm{Pr}, n, \lambda) = 0, \tag{13}$$

which are solved by a Chebyshev spectral collocation method. For the temporal linear stability analysis, we need to solve the problem of Eq. (13) for the given wave number α and β, while the frequency ω is complex and the imaginary part of ω represents the growth rate. Considering that all the variables are defined in the semi-infinite physical domain $y \in [0, \infty)$, so we map the computational Chebyshev domain $\eta \in [-1, +1]$ onto the physical domain via the coordinate transformation

$$y = \frac{L_{\max}}{2}(\eta + 1), \tag{14}$$

where $L_{\max}$ is the distance from the wall surface. Then, the eigenfunctions expanded in Chebyshev series are substituted into Eq. (13), which are applied at the Gauss-Lobatto points and solved by the QZ-method. For more details on numerical calculation, we refer the reader to Schmid and Henningson [29]. We take Several tests have for different Chebyshev points and computational domains to ensure numerical convergence, and the results are shown in Table I. Note that the results of Newtonian fluid ($n = 1$) are also listed in Table I, which is in good agreement with the results obtained by Xiao *et al.* [11] when using the same dimensionless parameters. The number of Chebyshev points $N = 100$ and the value of $L_{\max} = 30$ are found to be sufficiently accurate for all unstable modes discussed in this paper.

TABLE I. Numerical values of the frequency at different Chebyshev points and computational domains for four sets of typical parameters with $\mathrm{Pr} = 0.72$ and $\chi = 40^\circ$. The number of Chebyshev points 100 and $L_{\max} = 30$ are used in the following calculations, which is marked in bold.

(Gr, α, β)	$n = 0.6, \lambda = 1$ (50, 0.2, 0.2)	$n = 0.6, \lambda = 4$ (40, 0.4, 0.1)	$n = 1$ (41.26, 0.3578, 0)	$n = 1.2, \lambda = 8$ (60, 0.2, 0.8)
($L_{\max}$, N)	ω	ω	ω	ω
(15, 50)	3.0086–0.0255i	4.1099+0.2185i	3.6699+0.0633i	2.8853–0.0692i
(25, 50)	3.0127–0.0213i	4.1100+0.2187i	3.6704+0.0640i	2.8865–0.0695i
(30, 100)	**3.0127–0.0213i**	**4.1101+0.2187i**	**3.6704+0.0640i**	**2.8852–0.0692i**
(30, 200)	3.0127–0.0213i	4.1101+0.2187i	3.6704+0.0640i	2.8852–0.0692i
(50, 200)	3.0127–0.0213i	4.1101+0.2187i	3.6704+0.0640i	2.8852–0.0692i

III. RESULTS AND DISCUSSION

Since the linear instability problems play a significant role in the early stages of laminar-turbulent transition, a temporal stability analysis is carried out to predict the fastest growing perturbations in this section. The parametric study is mainly focused on the critical mode of the linear problem, and the following analysis in this part is focused mainly on the neutral curve by setting the complex-valued frequency $\omega_i = 0$. Temporal instabilities analysis of the dispersion relationship are based on the Grashof number Gr, streamwise and spanwise wave number α, β, Prandtl number Pr, tile angle χ, relaxation time λ, and power-law index n. Considering that it is extremely time-consuming and complicated to calculate in all parameter spaces, a typical value of λ is selected. However, some other values of λ are also calculated and no qualitative changes are found. The parametric study has been performed within the ranges $5^\circ < \chi < 90^\circ$, $10^{-2} < \mathrm{Pr} < 10^2$ and $n = 0.6, 0.8, 1, 1.2, 1.4$, with fixed $\lambda = 4$.

It should be noted that Eq. (10) have the following symmetry properties,

$$(\alpha, \beta, \omega) \to (\alpha, -\beta, \omega), \tag{15a}$$

$$(\alpha, \beta, \omega) \to (-\alpha, \beta, -\overline{\omega}), \tag{15b}$$

where $\overline{\omega}$ is the complex conjugate of ω. Considering those two symmetry properties, only cases with $\alpha > 0$ and $\beta > 0$ are calculated. For linear instability analysis, we show that in some parameter spaces several instability exchanges are noteworthy.

As mentioned in the Introduction, the instability of boundary layer may be dominated by three different modes, namely the transverse traveling Tolmien-Schlichting waves with $\beta = 0$ (TS mode), the stationary longitudinal rolls with $\alpha = 0$, $\omega_r = 0$ (SL mode) and the oblique roll with $\alpha \neq 0$, $\beta \neq 0$ (OR mode). To understand the influence of power law index n on different modes, we first select three typical values of $n = 0.6$, 1, and 1.4. The isocontours of Grashof number for different value of n with $\lambda = 4$, $\chi = 50^\circ$ and $\mathrm{Pr} = 0.72$ are illustrated in Fig. 3. Three typical modes, i.e., SL mode, OR mode and TS mode, are all reflected in isocontours. The stationary longitudinal rolls with zero frequency correspond to saddle points in α-β planes, which are not correspond to the local minimum. The descent from the saddle points always leads to a minimum of Gr related to OR mode or TS mode. In the case of shear-thinning fluid ($n = 0.6$) and Newtonian fluid ($n = 1$), the isocontours show similar characteristics, and the difference is only in quantity. As shown in Fig. 3(c), by browsing the isocontour, we find two local minimum of Gr correspond to OR mode for $n = 1.4$. It is worth mentioning that the coexistence of two OR modes is also mentioned in Tao's work [12] with Newtonian fluid and isoflux boundary condition. According to the value of streamwise wave number α, those two OR modes are referred to OR-1 and OR-2 in the following. The OR-1 mode with critical parameters $(\mathrm{Gr}, \alpha, \beta, \omega) = (43.428, 0.042, 0.343, 1.580)$ is nearly aligned with the streamwise direction, as α is about one order smaller than β. However, the critical

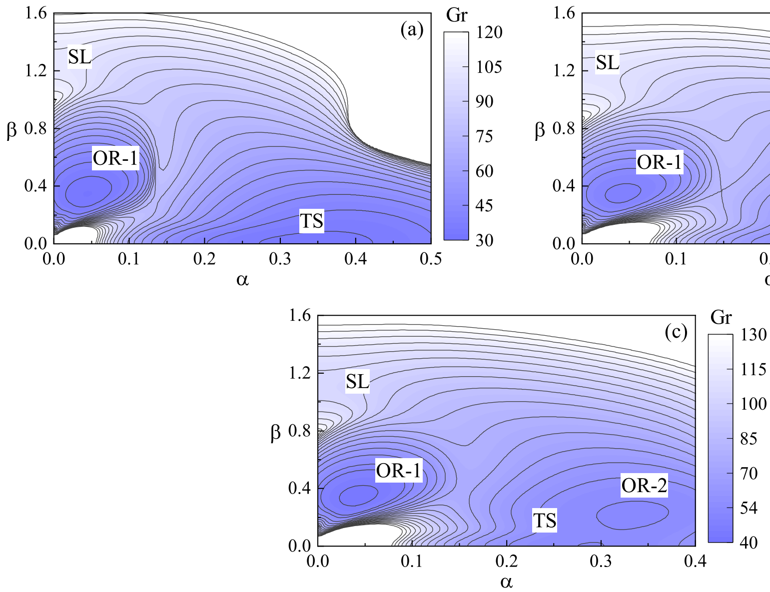

FIG. 3. Isocontours of the Gr for different value of power law index n, (a) $n = 0.6$, (b) $n = 1$, (c) $n = 1.4$, with $\lambda = 4$, $\chi = 50^{\circ}$, and Pr = 0.72. Higher Grashof numbers of neutral states are not shown, which are more stable modes and of lesser interest.

parameters for OR-2 are (Gr, α, β, ω) = (52.935, 0.335, 0.221, 3.665), which does not exist under the same tile angle and Prandtl number for Newtonian fluid and not reported before.

For dilatant fluid, the dependence on the Prandtl number of the critical parameter values for SL rolls, oblique rolls and TS waves are shown in Fig. 4 for $n = 1.4$ and $\chi = 60^{\circ}$. The critical Grashof numbers of all three modes decrease with increasing Prandtl number. The TS mode is the most stable mode until the Prandtl number increases to 0.33. TS mode has the smallest wave number near Pr = 1, and seems to have a asymptotic value when Prandtl number approaches zero. With the increase of Pr, the OR-2 and OR-1 modes become the most unstable modes in turn. The OR-2 mode exits in the range $0.33 < \mathrm{Pr} < 1$, and it is the most unstable mode only in a very small range

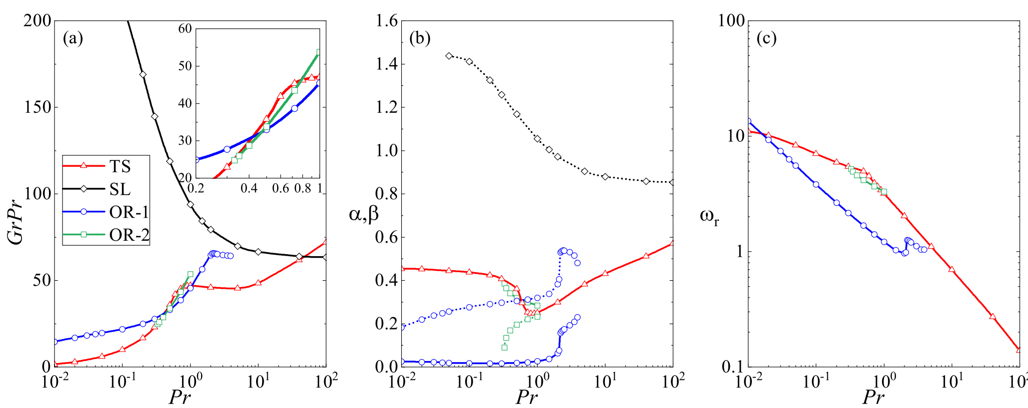

FIG. 4. The critical parameters (a) Grashof number, (b) wave number, and (c) frequency as functions of the Prandtl number Pr for $n = 1.4$ and $\chi = 60^{\circ}$. The critical wave numbers are given by the solid line (α) and the dotted line (β).

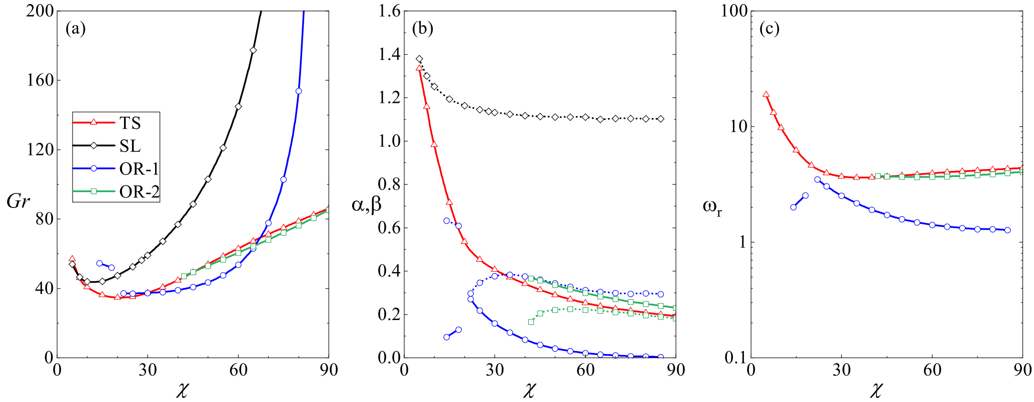

FIG. 5. The critical parameters (a) Grashof number, (b) wave number, and (c) frequency as functions of the tile angle χ for $n = 1.4$ and $\mathrm{Pr} = 0.72$. The critical wave numbers are given by the solid line (α) and the dotted line (β).

$0.33 < \mathrm{Pr} < 0.47$ [see the inset in Fig. 4(a)]. Until Pr is increased to 1.1, the most unstable mode changes back to TS wave, and the corresponding wave number increases with the increase of Pr, but the frequency decreases. The TS wave is characterized by the highest critical frequency except for $\mathrm{Pr} < 0.02$. For $\mathrm{Pr} > 3.9$, the critical oblique roll mode can no longer be found. With the further increase in Pr, for $\mathrm{Pr} > 48$, SL mode is the most unstable mode. However, the longitudinal roll has the largest critical wave number among the four modes and it decreases with increasing Prandtl number. It is interesting to note that when $\mathrm{Pr} \approx 2$, the local minimum corresponding to OR-1 mode moves rapidly in the α-β plane and disappear finally with increasing the Prandtl number.

For the inclined buoyancy layer, the tile angle χ should always be an important factor. Its influence on instability is discussed for $n = 1.4$ and $\mathrm{Pr} = 0.72$. As shown in Fig. 5(a), the critical Grashof numbers of SL rolls and TS wave first decrease and then increase, and each curve has a single minimum. When the tile angle is very small ($\chi < 7.2^\circ$), the plate is almost horizontal and the stationary convection rolls are dominant. Similar phenomenon has been reported by Tao [12] in Newtonian fluid. As the tile angle increases, TS waves are the most unstable mode when $7.2^\circ < \chi < 30^\circ$. In the range of $30^\circ < \chi < 66^\circ$, the critical mode changes to OR-1 mode. In

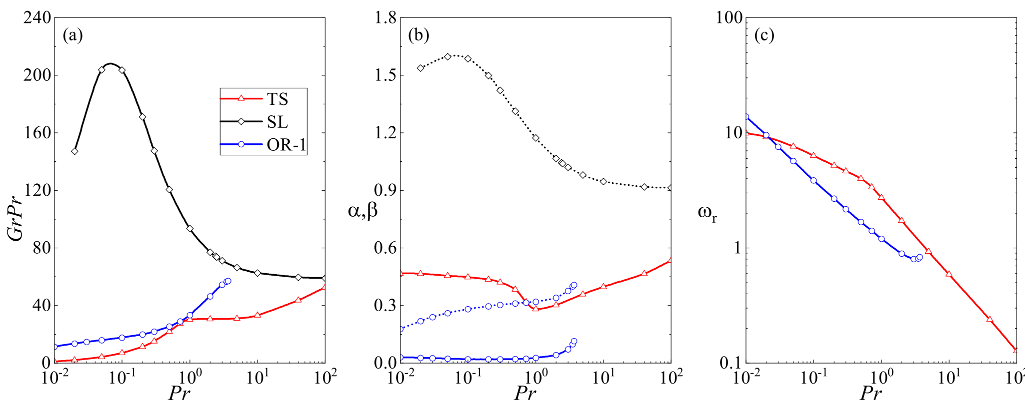

FIG. 6. The critical parameters (a) Grashof number, (b) wave number, and (c) frequency as functions of the Prandtl number Pr for $n = 0.6$ and $\chi = 60^\circ$. The critical wave numbers are given by the solid line (α) and the dotted line (β).

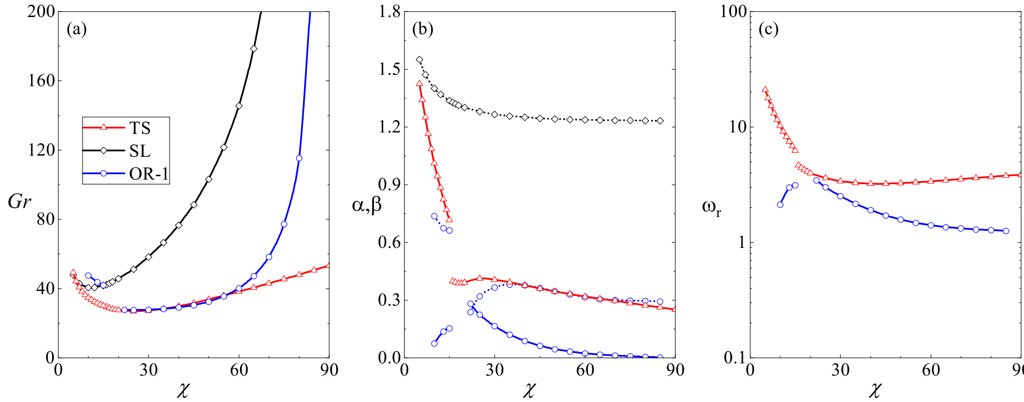

FIG. 7. The critical parameters (a) Grashof number, (b) wave number, and (c) frequency as functions of the tile angle χ for $n = 0.6$ and $\mathrm{Pr} = 0.72$. The critical wave numbers are given by the solid line (α) and the dotted line (β).

addition, OR-2 mode appears when $\chi > 42^\circ$, and with the further increase in tile angle, the Grashof number also increases gradually. Until χ is increased to 66°, the most unstable mode becomes OR-2 mode. The critical frequency and wave number are shown in Figs. 5(b) and 5(c), respectively. Under the same tile angle and Prandtl number, the frequency of OR-2 mode is higher than that of OR-1 mode.

For pseudoplastic fluid, the influence of the Prandtl number Pr on the properties of the most unstable mode for $n = 0.6$ and $\chi = 60^\circ$ is shown in Fig. 6. The similarity with the result of $n = 1.4$ is that the critical Grashof numbers of all three modes decrease with increasing Prandtl number. An important result obtained is that the curve for the oblique rolls mode does not intersect with that of the TS waves, and TS waves always become unstable first [see Fig. 6(a)]. Besides, the existence of OR-2 mode is not found at this tile angle, which is quite different from the result of dilatant fluids, and we have shown this feature in the isocontour of Fig. 3. Figures 6(b) and 6(c) plot the critical frequency and wave number, respectively. The dependence of instability on the tile angle in the case $\mathrm{Pr} = 0.72$ is illustrated in Fig. 7. The OR-2 mode is still not found in all the tile angles. TS waves set in first at most inclined angles except for $35^\circ < \chi < 56^\circ$ where the oblique roll is the most unstable mode. More importantly, the curves representing TS modes are discontinuous at $\chi = 15^\circ$, which is not obvious in Fig. 7(a), but the wave number curve in Fig. 7(b) clearly depicts this feature. This

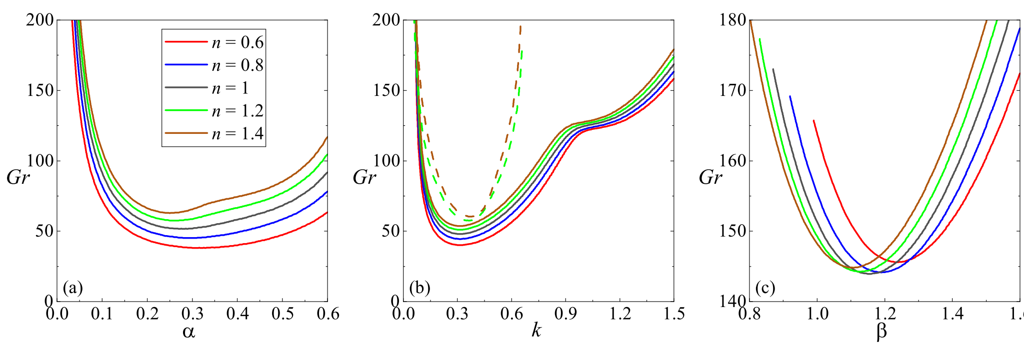

FIG. 8. The neutral curves for $\mathrm{Pr} = 0.72$ and $\chi = 60^\circ$ (a) TS mode, (b) OR mode, and (c) SL mode. For the oblique rolls mode, total wave number $k = (\alpha^2 + \beta^2)^{\frac{1}{2}}$ is used in abscissa. The OR-1 and OR-2 mode in panel (b) are represented by solid lines and dotted lines, respectively.

TABLE II. Critical values of Grashof number for different modes with $\mathrm{Pr} = 0.72$ and $\chi = 60^{\circ}$.

Mode	$n = 0.6$	$n = 0.8$	$n = 1.0$	$n = 1.2$	$n = 1.4$
TS	38.08	45.14	51.57	57.46	62.89
OR-1	40.13	44.44	47.98	51.03	53.68
OR-2	–	–	–	57.52	60.37
SL	145.59	144.15	143.94	144.25	144.81

phenomenon is not found in Newtonian fluid and dilatant fluid. In addition, as can be seen from the frequency curve shown in Fig. 7(c), the frequency corresponding to TS mode is always greater than that of OR mode. The longitudinal rolls mode represented by the black curve is always standing wave, so it is not shown.

The neutral stability curves obtained for TS mode, OR mode and SL mode are shown in Fig. 8. It can be seen that with the increase of power-law index n, the critical values of Grashof number Gr_c for TS waves increase, which means increasing n makes the basic flow more stable. However, the critical wave number α_c corresponding to Gr_c gradually decreases. For $n = 1.4$, the neutral curves exhibit the common feature in the buoyancy-driven system, i.e. the neutral curves have higher- and lower-wave-number parts. The nose-shaped piece are determined by thermal instability and mechanical instability. This feature is not significant when $n = 1$ and $\chi = 60^{\circ}$, but with the increase of fluid viscosity, the higher-wave-number part controlled by mechanical instability [3] gradually appears. For oblique rolls mode, the abscissa in Fig. 8(b) is expressed by the total wave number $k = (\alpha^2 + \beta^2)^{\frac{1}{2}}$. The results show that the critical Gr of both OR-1 and OR-2 modes increases with the increase of n, but there is no significant change in the critical wave number. Table II condenses the critical values of Grashof number shown in Fig. 8. Due to the large Gr_c, the SL mode is usually not the most unstable mode [see Fig. 8(c)]. Nevertheless, it is worth noting that both pseudoplastic fluid and dilatant fluid correspond to higher Gr_c compared with the case of Newtonian fluid. It suggests that the longitudinal rolls mode always becomes more stable regardless of the increase or decrease of the value of n.

IV. CONCLUSION

In this work, we have studied the linear instability of a non-Newtonian buoyancy-driven flow on an inclined heated plate in the stratified ambient fluid. The shear-thinning and shear-thickening behaviors of non-Newtonian fluids are described by the Carreau model. For basics flow, either increasing material time constant λ or decreasing power-law index n will promote convection. Based on the linear instability analysis regime with the coupled Orr-Sommerfeld equation and energy equation, the effects of Prandtl number Pr, tile angle χ and power-law index n are investigated. The present parametric study is mainly focused on the critical modes (TS waves, OR mode and SL mode) of the linear problem. For dilatant fluids ($n > 1$), a new oblique rolls mode appears under appropriate parameter, which is different from the result of Newtonian fluids. Several instability exchanges are identified for both dilatant fluid and pseudoplastic fluid. Depending on the tilt angle and the Prandtl number, the most unstable mode of a non-Newtonian buoyancy layers can be transverse TS waves, oblique rolls or stationary longitudinal rolls. Additionally, the neutral stability curves are obtained with different power-law index. Results suggest that the effect of shear-thickening will act to stabilize all the three modes, while the TS mode and OR mode are destabilized for shear-thinning.

However, for the parameter study in a large three-dimensional computational domain is rather time-consuming, only typical parameters are considered for temporal evolution of disturbance. It is conceivable that a situation where localized disturbance grows in both time and space. The present configuration can also be extended to analyze the spatial-temporal instability in buoyancy layer. For nonlinear instability, the effects of the nonlinear variation of the viscosity on the nature of the bifurcation are still an important subject. In addition, an inelastic non-Newtonian fluid is used in this paper, and the influence of elasticity of viscoelastic fluids on the stability of the boundary layer needs to be further studied. Despite this, we anticipate that the results may serve as a guide for future research in understanding such a non-Newtonian buoyancy-driven flow system.

ACKNOWLEDGMENTS

This work was supported by the National Natural Science Foundation of China (Grant No. 12072177) and the Natural Science Foundation of Shandong Province (Grants No. ZR2022QA090 and No. ZR2022MA033).

---

[1] L. Prandtl, *Essentials of Fluid Dynamics* (Blackie, London, 1952).
[2] A. E. Gill, The boundary-layer regime for convection in a rectangular cavity, J. Fluid Mech. **26**, 515 (1966).
[3] A. E. Gill and A. Davey, Instabilities of a buoyancy-driven system, J. Fluid Mech. **35**, 775 (1969).
[4] P. A. Iyer, Instabilities in buoyancy-driven boundary-layer flows in a stably stratified medium, Bound.-Layer Meteorol. **5**, 53 (1973).
[5] P. A. Iyer and R. E. Kelly, Supercritical solutions for the buoyancy boundary layer, ASME. J. Heat Transfer. **100**, 648 (1978).
[6] G. Desrayaud, Stability of flow near a heat-flux plate and comparison with numerical simulations in a square cavity, Report CNAM (1990).
[7] B. Gebhart, Y. Jaluria, R. L. Mahajan, and B. Sammakia, *Buoyancy-Induced Flows Transport* (Hemisphere, New York, 1988).
[8] G. D. McBain, S. W. Armfield, and G. Desrayaud, Instability of the buoyancy layer on an evenly heated vertical wall, J. Fluid Mech. **587**, 453 (2007).
[9] X. Xiong and J. Tao, Lower bound for transient growth of inclined buoyancy layer, Appl. Math. Mech.-Engl. Ed. **38**, 779 (2017).
[10] Y. Xiao, Y. Li, M. Zhao, and S. Wang, Finite-amplitude instability of the buoyancy boundary layer in a thermally stratified medium, J. Fluid Mech. **947**, A40 (2022).
[11] Y. Xiao, B. Zhang, M. Zhao, and S. Wang, Convective and absolute instabilities in inclined buoyancy layers, Phys. Fluids **34**, 094102 (2022).
[12] J. Tao and F. H. Busse, Oblique roll instability in inclined buoyancy layers, Eur. J. Mech. B Fluids **28**, 532 (2009).
[13] J. Candelier, S. LeDizès, and C. Millet, Inviscid instability of a stably stratified compressible boundary layer on an inclined surface, J. Fluid Mech. **694**, 524 (2012).
[14] L. Krizhevsky, J. Cohen, and J. Tanny, Convective and absolute instabilities of a buoyancy-induced flow in a thermally stratified medium, Phys. Fluids **8**, 971 (1996).
[15] J. Tao, P. LeQuéré, and S. Xin, Absolute and convective instabilities of natural convection flow in boundary-layer regime, Phys. Rev. E **70**, 066311 (2004).
[16] J. Tao, P. LeQuéré, and S. Xin, Spatio-temporal instability of the natural-convection boundary layer in thermally stratified medium, J. Fluid Mech. **518**, 363 (1999).
[17] Y. Xiao, B. Zhang, M. Zhao, and S. Wang, Instabilities of buoyancy-induced flow along vertical cylinder in thermally stratified medium, Phys. Fluids **34**, 044109 (2022).
[18] D. A. Siginer, D. De. Kee, and R. P. Chhabra, Advances in the flow and rheology of non-Newtonian fluids parts A & B, J. Non-Newtonian Fluid Mech. **91**, 298 (2000).
[19] H. Ozoe and S. W. Churchill, Hydrodynamic stability and natural convection in Ostwald-de Waele and Ellis fluids: The development of a numerical solution, AIChE J. **18**, 1196 (1972).
[20] M. M. Molla and L. S. Yao, Non-Newtonian natural convection along a vertical plate with uniform surface heat fluxes, J. Thermophys. Heat Transfer **23**, 176 (2009).

[21] M. Kaddiri, M. Naïmi, A. Raji, and M. Hasnaoui, Rayleigh-Bénard convection of non-Newtonian power-law fluids with temperature-dependent viscosity, ISRN Thermodyn. **2012**, 614712 (2012).

[22] Z. Alloui, N. Ben Khelifa, H. Beji, P. Vasseur, and A. Guizani, The onset of convection of power-law fluids in a shallow cavity heated from below by a constant heat flux, J. Non-Newtonian Fluid Mech. **196**, 70 (2013).

[23] P. J. Carreau, Rheological equations from molecular network theories, J. Rheol. **16**, 99 (1972).

[24] P. T. Griffiths, M. T. Gallagher, and S. O. Stephen, The effect of non-Newtonian viscosity on the stability of the Blasius boundary layer, Phys. Fluids **28**, 074107 (2016).

[25] P. T. Griffiths, Stability of the shear-thinning boundary-layer flow over a flat inclined plate, Proc. R. Soc. A. **473**, 20170350 (2017).

[26] F. Rousset, S. Millet, V. Botton, and H. B. Hadid, Temporal stability of Carreau fluid flow down an incline, J. Fluids Eng. **129**, 913 (2007).

[27] R. Rebhi, M. Mamou, and N. Hadidi, Bistability bifurcation phenomenon induced by non-Newtonian fluids rheology and thermosolutal convection in Rayleigh-Bénard convection, Phys. Fluids **33**, 073104 (2021).

[28] R. B. Bird, R. C. Armstrong, and O. Hassager, *Dynamics of Polymeric Liquids, Volume 1: Fluid Mechanics*, 2nd ed. (Wiley, New York, 1987).

[29] P. J. Schmid and D. S. Henningson, *Stability and Transition in Shear Flows* (Springer, Berlin, 2001).